Title

Strikingly High Activity of 15-Lipoxygenase Towards Di-Polyunsaturated Arachidonoyl/Adrenoyl-Phosphatidylethanolamines Generates Peroxidation Signals of Ferroptotic Cell Death

Authors

Samovich, Svetlana N
Mikulska-Ruminska, Karolina
Dar, Haider H
et al.

Publication Date

2024-01-17

DOI

10.1002/anie.202314710

Strikingly High Activity of 15LOX Towards Di-Polyunsaturated Arachidonoyl/Adrenoyl-Phosphatidylethanolamines Generates Peroxidation Signals and Sensitizes Cells to Ferroptotic Death

S.N. Samovich[a,b], K. Mikulska-Ruminska[c], H.H. Dar[b], Y.Y. Tyurina[b], V.A. Tyurin[b], Austin B. Souryavong[b], A.A. Kapralov[b], A.A. Amoscato[b], O. Beharier[d], S.A. Karumanchi[e], C.M. St. Croix[f], X. Yang[g], T.R. Holman[h], A.P. VanDemark[i], Y. Sadovsky[j,k], R.K. Mallampalli[l,m], S.E. Wenzel[b], W. Gu[g,n], Y.L. Bunimovich[b,o], I. Bahar[p], V.E. Kagan*[b,m,q,r], H. Bayir*[a,b,s]

[a] Department of Pediatrics, Division of Critical Care and Hospital Medicine, Redox Health Center, Vagelos College of Physicians and Surgeons, Columbia University Irving Medical Center, New York, NY 10032, USA.
[b] Department of Environmental and Occupational Health, Center for Free Radical and Antioxidant Health, School of Public Health, University of Pittsburgh, Pittsburgh, PA 15261, USA.
[c] Institute of Physics, Faculty of Physics Astronomy and Informatics, Nicolaus Copernicus University in Torun, Torun PL87100, Poland.
[d] Obstetrics and Gynecology Division, Hadassah Medical Center, Faculty of Medicine of the Hebrew University of Jerusalem, Jerusalem, Israel.
[e] Department of Medicine, Cedars-Sinai Medical Center, Los Angeles, CA 90048, USA.
[f] Department of Cell Biology, University of Pittsburgh, Pittsburgh, PA 15260, USA.
[g] Institute for Cancer Genetics, and Herbert Irving Comprehensive Cancer Center, Vagelos College of Physicians and Surgeons, Columbia University, New York, NY 10032, USA.
[h] Department of Chemistry and Biochemistry, University of California Santa Cruz, Santa Cruz, CA 95064, USA.
[i] Department of Biological Sciences, University of Pittsburgh, Pittsburgh, PA 15213, USA.
[j] Magee-Womens Research Institute, Department of Obstetrics, Gynecology, and Reproductive Sciences, University of Pittsburgh, Pittsburgh, PA 15213, USA.
[k] Department of Microbiology and Molecular Genetics, University of Pittsburgh, Pittsburgh, PA 15219, USA.
[l] Department of Medicine, University of Pittsburgh, Pittsburgh, PA 15213, USA.
[m] Department of Radiation Oncology, University of Pittsburgh, Pittsburgh, PA 15213, USA.
[n] Department of Pathology and Cell Biology, Vagelos College of Physicians and Surgeons, Columbia University, New York, NY 10032, USA.
[o] Department of Dermatology, University of Pittsburgh, Pittsburgh, PA 15213, USA.
[p] Laufer Center for Physical and Quantitative Biology, Laufer Center, Z-5252, Stony Brook University, Stony Brook, NY, 11794, USA.
[q] Department of Chemistry, University of Pittsburgh, Pittsburgh, PA 15260, USA.
[r] Department of Pharmacology and Chemical Biology, University of Pittsburgh, Pittsburgh, PA 15261, USA.
[s] Department of Critical Care Medicine, Safar Center for Resuscitation Research, Children's Neuroscience Institute, Children's Hospital of Pittsburgh, University of Pittsburgh, Pittsburgh, PA 15213, USA.

KEYWORDS: ferroptosis; 15-lipoxygenase; doubly PUFA-acylated phosphatidylethanolamines, redox lipidomics

ABSTRACT: The vast majority of membrane phospholipids (PLs) include two asymmetrically positioned fatty acyls: oxidizable polyunsaturated fatty acids (PUFA) attached predominantly at the sn2 position, and non-oxidizable saturated/monounsaturated acids (SFA/MUFA) localized at the sn1 position. The peroxidation of PUFA-PLs, particularly sn-2-arachidonoyl(AA)- and sn2-adrenoyl(AdA)-containing phosphatidylethanolamines (PE), has been associated with the execution of ferroptosis, a program of regulated cell death. There is a minor subpopulation (~1-2 mol%) of doubly PUFA-acylated phospholipids (di-PUFA-PLs) whose role in ferroptosis remains enigmatic. Here we report that 15-lipoxygenase (15LOX) exhibits unexpectedly high pro-ferroptotic peroxidation activity towards di-PUFA-PEs. We revealed that peroxidation of several molecular species of di-PUFA-PEs occurs early in ferroptosis. Ferrostatin-1, a typical ferroptosis inhibitor, effectively prevented peroxidation of di-PUFA-PEs. Furthermore, co-incubation of cells with di-AA-PE and 15LOX produced PUFA-PE peroxidation and induced ferroptotic death. The decreased contents of di-PUFA-PEs in ACSL4 KO A375 cells was associated with lower levels of di-PUFA-PE peroxidation and enhanced resistance to ferroptosis. Thus, di-PUFA-PE species are newly identified phospholipid peroxidation substrates and regulators of ferroptosis, representing a promising therapeutic target for many disease conditions related to ferroptotic death.

Introduction

Ferroptosis is a recently identified type of regulated cell death program executed via (phospho)lipid peroxidation triggered by dysregulated redox-active iron and insufficient thiol control.[1] In ferroptosis, peroxidation occurs on a larger scale than in any other described cell death program, both in terms of the amounts of products and types of peroxidized lipid species, championed by arachidonoyl- and adrenoyl-phosphatidylethanolamines (PEs).[2] Insufficient

amounts of readily peroxidizable polyunsaturated fatty acid (PUFA)-containing phospholipids (PLs) have been shown to suppress ferroptosis; conversely, supplementation of cells with peroxidation-prone PUFA, such as arachidonic acid, accelerates ferroptotic cellular demise. In line with this, several genes and their corresponding products regulating PUFA-containing PLs have been identified as regulators of ferroptotic death, including ACSL4, LPCAT3, FATP2, MBOAT1/2.[3,4,5] Paradoxically, although the availability of PUFA-PLs has been recognized as a universal mechanism of ferroptosis regulation, the amounts of peroxidation products accumulating in ferroptosis are ~two orders of magnitude lower than the total levels of the respective oxidizable substrates. PUFA-residues are typically located in sn2 positions of PLs although there are also doubly-PUFA PLs (di-PUFA-PLs), albeit at much lower abundance. Redox lipidomics of these di-PUFA-PLs in ferroptosis has not been studied.

Three major types of products are formed during lipid peroxidation process: i) hydroperoxy-PLs (HOO-PLs during the initiation), ii) oxidatively-truncated electrophilic species (secondary products) of HOO-PLs breakdown, and iii) covalent adducts of the oxidatively-truncated PLs with proteins leading to protein lipoxidation.[6,7] Selective and specific peroxidation and production of HOO-PUFA-phosphatidylethanolamines (HOO-PUFA-PEs) during the initiation of ferroptosis is catalyzed by lipoxygenases (LOXs), particularly by 15LOX.[8,9]

Lipoxygenases (LOXs) represent a family of non-heme iron proteins catalyzing the oxygenation of *free* polyunsaturated fatty acids (PUFA), most commonly arachidonic acid (AA, eicosatetraenoic acid, ETE, C20:4).[10] This reaction yields a variety of products – lipid mediators – with a broad spectrum of biological effects.[11] Organization of the LOX catalytic site defines the position and stereospecificity of the substrate oxygenation by the members of the LOX family. Precise catalytic H-abstraction from bis-allylic carbons necessitates their position juxtaposed to the catalytic iron, thus reflecting the nomenclature of 5-, 8-, 12-, 15-LOXs.[12]

Most of mammalian LOXs do not typically peroxidize PUFA esterified into PLs with the notable exception of 12- and 15-LOXs,[10] which generate the respective 12- and 15-hydroperoxy-AA-PLs (12-/15-HOO-AA-PEs), albeit at more than an order of magnitude lower rates compared to the peroxidation of free PUFA. Several possible mechanisms may account for this difference, among them the known fact that PLs typically contain poorly oxidizable saturated or monounsaturated fatty acids (FA) lacking bis-allylic carbons at the sn1 position, while readily oxidizable PUFA residues are present at the sn2 position.[8,13] If a non-oxidizable FA non-productively occupies a position in the proximity of the catalytic Fe, the overall peroxidation rate may be low. Vice versa, when sn2 readily oxidizable PUFA residues are properly oriented, their oxidation proceeds without any hindrances. Obviously, this limitation does not apply to di-PUFA-PLs, which are rare molecular species with two oxidizable PUFA residues. We hypothesized that such di-PUFA-containing PLs will undergo peroxidation at significantly higher rates, primarily due to the lack of non-productive enzyme/substrate complexes. From a biological standpoint, this would mean that di-PUFA-PLs may represent preferred substrates for peroxidation reactions during the initiation of ferroptosis.

In the current work, we used biochemical, cell biological, computational and redox lipidomics protocols to explore oxidation of di-PUFA-PLs. We discovered that di-PUFA-PEs are oxidized by 15LOX at strikingly higher (~14-fold) rates than mono-PUFA-PEs. Molecular dynamics (MD) simulations confirmed that this difference is mainly caused by the lack of non-productive enzymatic complexes where non-oxidizable SFA/MUFA-residues are positioned in the proximity of the catalytic Fe. The regulatory effects of PEBP1, a scaffold protein characteristic of 15LOX-catalyzed mono-PUFA-PE oxidation, are not observed during di-PUFA-PE peroxidation. We further established that di-PUFA-PEs are preferably oxidized by 15LOX in mixtures of natural brain PLs as well as in several different types of cells. Elevated levels of di-PUFA-PEs and increased sensitivity to ferroptosis were observed in wild-type (WT) cells, but not in ACSL4-deficient cells.

Results

We opted to comparatively assess the contents of di-PUFA-PLs *vs.* mono-PUFA-PLs in several cell lines, focusing specifically on the most abundant AA- and adrenoyl (AdA, docosatetraenoyl, C22:4)-containing PLs, namely phosphatidylcholines (PCs) and PEs (**Figure 1**). These estimates showed that the amounts of mono-PUFA-PLs were, on average, 1-2 orders of magnitude higher than di-PUFA-PLs and

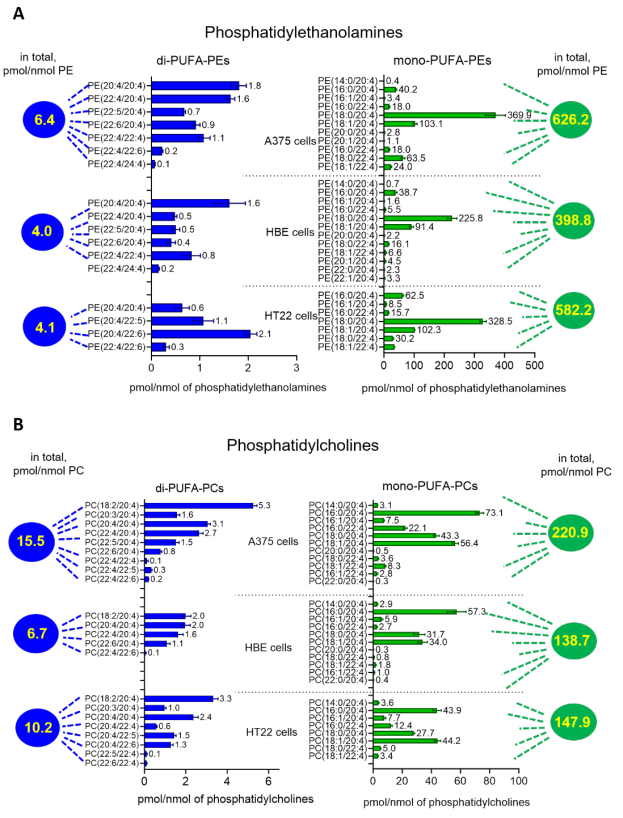

Figure 1. Content of AA and AdA-containing di-acyl **(A)** PE and **(B)** PC species in Human melanoma cells (A375), Human Bronchoalveolar cells (HBE) and mouse Hippocampal Neuronal cells (HT22). Data are expressed as pmol/nmol of PL classes. Data are mean ± s.d., n = 3.

this difference was much larger for PE>>PC.

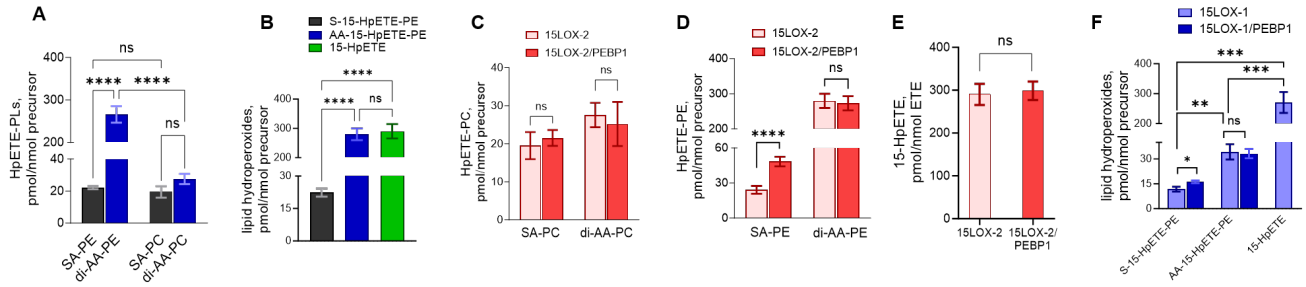

Figure 2. Oxidation of PE and PC by 15LOX or 15LOX/PEBP1 complex in liposomes prepared from a mixture of PLs. (**A**) Content of 15-HpETE-PE (15-HpETE-PC) molecular species accumulated during the oxidation of PE (PC) containing liposomes by 15LOX-2. Data are mean ± s.d., n = 4-5, **** p<0.0001, One-way ANOVA, Tukey's multiple comparisons test. (**B**) Accumulation of S-15-HpETE-PE (black bar), AA-15-HpETE-PE (blue bar) and 15-HpETE (green bar) in the presence of 15LOX-2. Data are mean ± s.d., n = 8, **** p<0.0001, One-way ANOVA, Tukey's multiple comparisons test. **(C)** Accumulation of S-15-HpETE-PE, AA-15-HpETE-PE and 15-HpETE in the presence of 15LOX-1 (blue bar) or 15LOX-1/PEBP1 complex (dark blue bar). Data are mean ± s.d., n = 3,***. p<0.0005, ** p<0.005,* p<0.05, student's t-test. Accumulation of HpETE-PC (**D**), HpETE-PE (**E**) and 15-HpETE **(F)** in the presence of 15LOX-2 (red bar) or 15LOX-2/PEBP1 complex (dark red bar). Data are mean ± s.d., n = 4-8, **** p<0.0001, student's t-test.

The higher levels of di-PUFA-PCs potentially make them favorable candidates for pro-ferroptotic peroxidation. Given that PCs and PEs are two preponderant PL classes of membranes and assuming the important role of 15LOX in the initiation of pro-ferroptotic peroxidation, we comparatively assessed the oxygenation of mono- and di-PUFA-PCs and PEs by 15LOX-2, a commonly occurring 15LOX isoform. Specifically, sn1-stearoyl-sn2-arachidonoyl-PE (SA-PE), sn1-stearoyl-sn2-arachidonoyl-PC (SA-PC) as well as 1,2-di-arachidonoyl-PE (di-AA-PE) and 1,2-di-arachidonoyl-PC (di-AA-PC) were examined (**Figure 2**). Interestingly, 15LOX-2 demonstrated similar low effectiveness in oxygenating SA-PC and SA-PE (**Figure 2A**). Di-AA-PC was oxidized at approximately the same rate as SA-PC – which is ~14 times slower than peroxidation of free AA (**Figure 2B**). In sharp contrast, 15LOX-2 catalyzed di-AA-PE oxidation 13.6-fold faster than SA-PE, with a rate comparable to that of free AA oxidation (**Figure 2B**). Peroxidation of "canonical" PEs and generation of the pro-ferroptotic signal, 15-HOO-AA-PE (15-HpETE-PE), is executed by a complex of 15LOX-2 with a scaffold protein, PEBP1.[9] In a biochemical model, PEBP1 did not accelerate the peroxidation of either SA-PC or di-AA-PC (**Figure 2C**). However, PEBP1 caused a two-fold increase in SA-PE oxidation rate (**Figure 2D**). When di-AA-PE was used as a substrate, PEBP1 did not affect the oxidation rate. Similarly, the oxidation of free AA was not affected by PEBP1 (**Figure 2E**). The selectivity of the PE oxidation was also found for 15-lipoxygenase-1 (15LOX-1). However, in this case, the oxidation rate of di-AA-PE was only 3-fold higher than for SA-PE and still 8-fold lower than that of free AA (**Figure 2F**). Similar to 15LOX-2, these characteristic features of di-AA-PE peroxidation by 15LOX-1 were insensitive to the presence of PEBP1 (in contrast to a 1.4-fold simulation of SA-PE oxidation rate by the 15LOX-1/PEBP1 complex) (**Figure 2F**).

Given the robust differences in the effectiveness of oxidation of SA-PE vs di-AA-PE, we further performed LC-MS/MS analysis of products resulting from their enzymatic oxidation (**Figure 3, Supplementary Figure 1**). SA-PE, which contains only one oxidizable FA, was found to

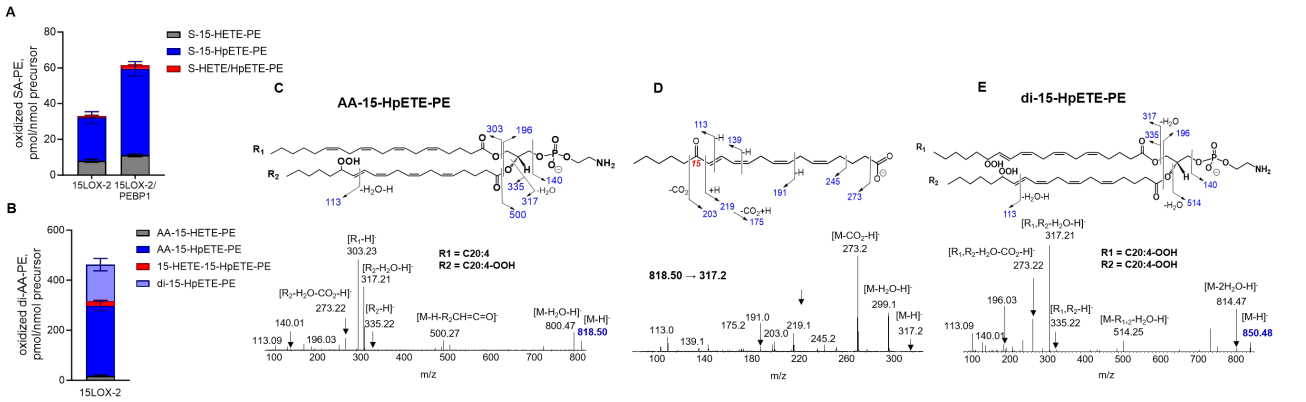

Figure 3. LC-MS/MS identification of oxidized SA-PE and di-AA-PE molecular species accumulated during incubation of liposomes with 15LOX-2 or 15LOX-2/PEBP1 complex. Content of **(A)** SA-PE and **(B)** di-AA-PE oxidized species accumulated in a model system. Data are mean ± s.d., n = 8. **(C)** Typical MS2 spectrum (left) of AA-15HpETE-PE (m/z 818.50) containing AA (C20:4, m/z 303.23) and AA-OOH (molecular ion with m/z 317.22 is corresponding to C20:4-OOH – H_2O). Upper left inset, structural formula of AA-15-HpETE-PE and corresponding fragments. **(D)** Typical MS3 spectrum of esterified AA-OOH to AA-15-HpETE-PE after loss of water molecule. Upper inset, structural formula of molecular ion with m/z 317.3 and corresponding fragments. Fragments with m/z 273.2 formed by loss of CO_2 from the carboxylate anion; m/z 299.1 originating from the carboxylate anion after loss of water molecule; m/z 219.1 fragment is generated via C14-C15 bond cleavage, m/z 139.1 is formed after the cleavage at C11-C12 double bond. The fragment with m/z 113.0 is produced after C13-C14 double bond cleavage and is indicative of the OOH-group at 15th carbon of the ketone group formed after loss of water molecule from AA-15-HpETE-PE. (**E**) Typical MS2 spectrum (right) of di-15-HpETE-PE (m/z 850.48) containing two AA-OOH (molecular ion with m/z 317.2 is corresponding to C20:4-OOH – H_2O). Upper right inset, structural formula of di-15-HpETE-PE and corresponding fragments.

predominantly yield S-15-HpETE-PE as the major product (72.7±1.9mol%), with lesser amounts of S-15-HO-AA-PE (S-15-HETE-PE) (24.3±1.9mol%) and S-HETE/HpETE-PE (3.0±0.8mol%) (**Figure 3A**). Hydroxy- and hydroperoxy-groups where present in the sn2 AA-residue (**Supplementary Figure 1A**). PEBP1 strongly affected the accumulation of S-15-HpETE-PE but not of S-15-HETE-PE. Di-AA-PE was oxidized to yield mono-HOO-AA-PE (AA-15-HpETE-PE) as the quantitatively dominating product (60.7±2.9mol%) (**Figure 3B,C,D, Supplementary Figure 1B**). However, di-HOO-AA-PE (di-15-HpETE-PE) was also generated and accounted for 31.3±2.6mol% of total oxidized products (**Figure 3B,E, Supplementary Figure 1B**). Notably, the products with two HOO-groups in both sn1-AA and sn-2 AA-residues of di-AA-PE were formed accounting for 28.6±0.9mol% of all di-15-HpETE-PE, whereas less than 2.6±0.9mol% of the products with both HOO-groups were present in the same AA-residue (**Supplementary Figure 1C**). Only small amounts of a hydroxy-product - AA-15-HO-AA-PE (AA-15-HETE-PE) and mixed species HpETE-HETE-PE, both featuring oxidized sn1-AA and sn-2 AA-residues, were detected at levels of 3.8±0.6mol% and 4.1±0.7mol%, respectively. (**Figure 3B, Supplementary Figure 1A**). LC-MS/MS analysis revealed that the 15LOX-2 oxidation of SA-PE and di-AA-PE displayed high positional specificity, with the 15-isomer being the dominant product generated at not exceeding the 9.8:0.2 ratio vs. 12-HpETE-PE (**Figure 3D, Supplementary Figure 1D**).

To explain the differences in the oxidation rates and the supportive role of PEBP1, exclusively for oxidation of SA-PE, we next performed computational modeling. MD simulations showed that SA-PE can bind 15LOX-2 either through oxidizable or non-oxidizable FA residues (**Figure 4A**).

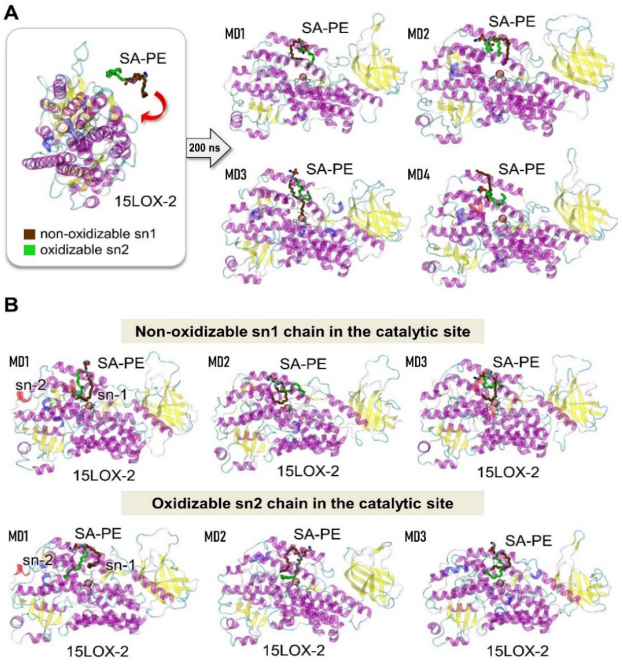

Figure 4. Substrate's dynamics and binding sites on 15LOX-2 identified in MD simulations. **(A)** Final conformations of SA-PE after 200 ns MD simulations. In the inset the initial conformation of the system. **(B)** SA-PE binding poses after 500-ns independent runs (MD1-3) with non-oxidizable sn-1 (*upper panel*) and oxidizable sn-2 (*lower panel*) FA bound at the catalytic site.

Examination of the stability of FA-residues interactions at the catalytic site confirmed the long-term association of both conformations (**Figure 4B**, see **Movie 1**). Thus, non-productive occupancy of the catalytic site by the non-oxidizable FA-residue of SA-PE can delay the peroxidation process. This "competition" between oxidizable and non-oxidizable FA residues occurred in the absence of PEBP1, occasionally leading to disruption of the oxidizable conformation (see **Movie 2**). The non-productive conformation was not observed in the presence of PEBP1 (**Figure 5A**, **Movie 3, and Supplementary Figure 2A**), thus explaining a significantly higher oxidation rate of SA-PE in its presence (**Figure 2**). In contrast, PEBP1 did not affect di-AA-PE interactions with the 15LOX-2 catalytic site (**Figure 5B, Supplementary Figure 2A-B**). The sn-1 AA-residue of di-AA-PE was not attracted by PEBP1 which stayed close to the α2 helix of 15LOX-2 (*red oval* and **Movies 4-6**). The conformation of the sn-2 AA-residue of di-AA-PE buried in the catalytic site was not affected by PEBP1: the distance between the bis-allylic C13 carbon atom and the catalytic iron remained unchanged in the presence and absence of PEBP1 (**Figure 5C**).

To assess whether di-AA-PE and other doubly-PUFA-PE (di-PUFA-PE) species are preferentially oxidized by 15LOX-2 in a natural mixture of PLs, we employed liposomes prepared

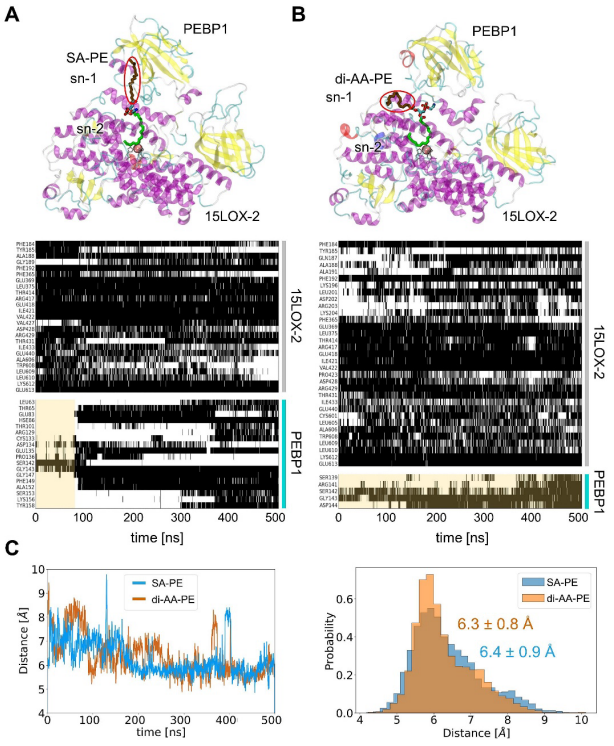

Figure 5. 15LOX-2/PEBP1 complex interactions with substrates observed in MD simulations. Final conformations of the complex with bound SA-PE **(A)** and di-AA-PE **(B)**. The time evolution of contacts between 15LOX-2/PEBP1 residues and substrates are also displayed (distance < 3.5 Å). Contacts are shown by black shades/bars for each residue. Orange shade denotes similar interactions with PEBP1 for SA-PE and di-AA-PE at the beginning of simulations. **(C)** Time evolution plot of the distance between C13 of di-AA-PE or SA-PE (containing bis-allylic hydrogen for the peroxidation process) and catalytic iron. Histogram of distances for both systems. Mean value and standard deviation for C13-Fe^{3+} distances are shown.

from a mixture of all PE species extracted and purified from mouse brain tissue (**Figure 6**). This assortment of natural PEs included 69 mol% of sn1-SFA/MUFA-sn2-PUFA-PE (33 individual species), 29.8 mol% of poorly oxidizable SFA/MUFA in both sn1 and sn2 residues (16 individual species), and only 1.2 mol% of di-PUFA-PEs (10 individual species) (**Figure 6B, Supplementary Table 2**). Notably, di-PUFA-PEs were oxidized at higher rates than sn1-SFA/MUFA-sn2-PUFA-PEs when all PE species were present in the mixture (**Figure 6C**). Specifically, the oxidation rate of di-AA-PE by 15LOX-2 was on average 2-fold higher than that of SA-PE, with 25 mol% of di-AA-PE being consumed compared to 8 mol% of SA-PE by the oxidation reaction (**Figure 6A**). This was determined by considering that the ratio of SA-PE to di-AA-PE was 99.7:0.3 in the prepared liposomes. Similar to oxidation of SA-PE in SA-PE:DOPC liposomes, PEBP1 was effective in accelerating peroxidation of sn1-SFA/MUFA-sn2-PUFA-PE species in the liposomal mixture (**Figure 6D**) – in contrast to oxidation of di-PUFA-PE species in the liposomal mixture that was not stimulated by PEBP1.

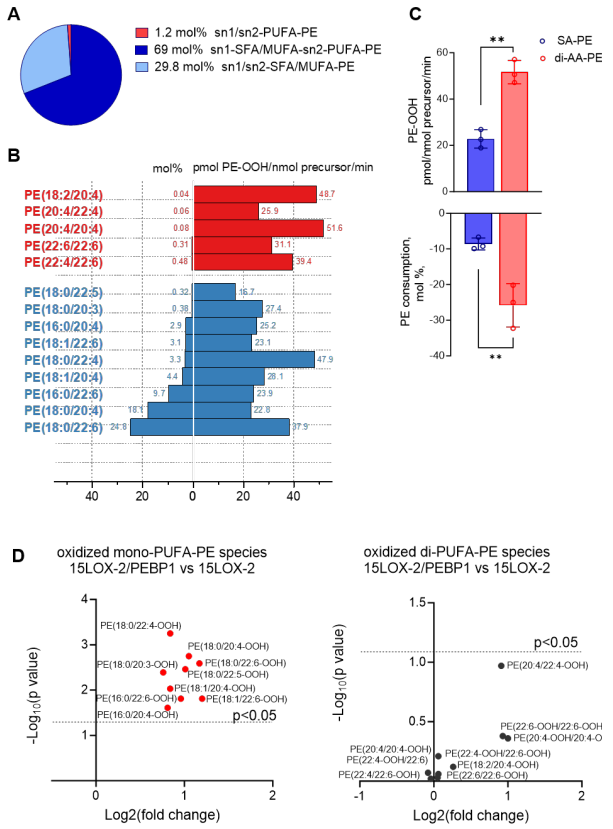

Figure 6. Oxidation of PE species by 15LOX-2 or 15LOX-2/PEBP1 complex in liposomes prepared from a natural PE mixture. (**A**) Rates of di-AA-PE and SA-PE oxidation and mol% of their consumption in the presence of 15LOX-2 during the oxidation reaction. Data are mean ± s.d., n = 3. ** p<0.005, student's t-test. (**B**) Content of PE species in a biochemical model containing natural mixture of PEs. (**C**) Rates of 15LOX-2 catalyzed oxidation of di-PUFA-PEs and sn1-SFA/MUFA-sn2-PUFA-PEs and their content in a biochemical model containing natural mixture of PEs (**D**) Volcano plots of 15LOX-2/PEBP1 vs 15LOX-2 induced changes of oxidized mono-PUFA-PEox (left plot) and di-PUFA-PEox (right plot), (log2 fold change) versus significance (log10 p value). Data are expressed as pmol/nmol PEs.

We next asked whether the discovered specific features of di-AA-PE oxidation are translated into biologically significant effects. To this end, we developed and employed a new model utilizing 15LOX-2 for oxidation of different exogenously added PLs, particularly SA-PE and di-AA-PE, to trigger the ferroptotic response in cells. We used human bronchoalveolar cells (HBE) cells treated with a low concentration of a GPX4 inhibitor, RSL3, to prevent cellular reduction of HpETE-PEs into their respective alcohols.[14] We chose conditions in which RSL3 alone caused 22.4±2.6% cell death vs. control (non-exposed to RSL3). A combination of RSL3 with 15LOX-2 plus di-AA-PE containing liposomes under the same conditions caused 77.0±5.7% cell death (and an increase in 54.6±4.1% over the effect of RSL3 alone) (**Figure 7A**). Cellular demise was due to ferroptosis as its specific inhibitors, ferrostatin-1 (Fer-1) and liprostatin-1 (Lip-1), completely blocked cell death, whereas inhibitors of necroptosis (necrostatin-1S, Nec-1S) and apoptosis (zVAD-fmk) did not demonstrate any significant protection or displayed only marginal levels of protection (**Figure 7A).** Under the same conditions, the combination of RSL3, 15LOX-2, and SA-PE resulted in 27.4±1.5% cell death, indicating only a 5.0±2.1% increase compared to the effect of RSL3 alone. Finally, we demonstrated that the oxidation of exogenously added di-AA-PE plus 15LOX-2 sensitized several cell lines to RSL3-induced ferroptosis, namely human HaCaT keratinocyte cells and A375 melanoma cells (**Figure 7B, Supplementary Figures 3,4**). In HaCaT cells, the oxidation of di-AA-PE by 15LOX-2 led to 41.6±3.1% cell death, demonstrating a significant 32.0±1.9% increase compared to the effect observed with RSL3 alone. Furthermore, the addition of SA-PE resulted in 25.1±4.1% cell death, indicating only a 15.5±2.4% increase compared to the effect of RSL3 alone (**Figure 7B**). In A375 melanoma cells, the combination of di-AA-PE plus 15LOX-2 demonstrated significantly lower viability compared to RSL3 alone (40.8±2.9% compared to 75.3±3.2%, respectively). Conversely, the presence of SA-PE+15LOX-2 did not result in a significant change in cell viability (73.8±4.4%) compared to RSL3 alone (**Supplementary Figure 3A**). Additionally, we investigated di-AA-PC-induced ferroptosis in A375 cells and observed no significant change in cell viability (72.2±1.5%) compared to RSL3 alone (**Supplementary Figure 3B**). This corresponds with di-AA-PC being a poor substrate for the enzyme. These findings support the idea of the unique and high activity of 15LOX-2 towards di-PUFA-PE species in inducing ferroptosis. Assuming that ferroptotic death was due to the effects of HOO-PEs, we chose to examine whether pre-synthesized (using 15LOX-2) 15-HpETE-PEs would also cause quantitatively comparable effects on cells. Interestingly, we found that mono-HOO-PE, AA-15HpETE-PE, was effective in inducing ferroptotic death (**Figure 7C**). The effect of di-15HpETE-PE was strikingly different; no cell death over RSL3-induced effect was observed when HOO-groups were present in both sn1-AA and sn2-AA residues of di-HpETE-PE. This may be explained by very high solubility of doubly oxygenated di-15HpETE-PE with both AA-residues having a polar HOO-group. Indeed, we found that di-HpETE-PE is water-soluble and did not bind membranes but instead could be recovered from the supernatant

(**Supplementary Figure 4**). During lipid peroxidation, not only reactive radical intermediates, but also molecular products – HOO-lipids and electrophilic oxidatively-truncated species generated from HOO-PLs form covalent adducts with proteins.[6] Because of the transient nature of PLs peroxidation products, the totality of their redox reactions may be better characterized by quantitative assessments of changes in the oxidizable substrates, PUFA-PLs. Indeed, our redox lipidomics analysis of HBE cells revealed the changes in the levels of oxidizable di-PUFA vs mono-PUFA AA-/AdA-containing PE species after 4h incubation in the presence of RSL3±15LOX-2+di-AA-PE (**Figure 7D**). Notably, the levels of several di-PUFA-PE species were markedly (by 12.5±5.1% – 40.0±6.4%) decreased under these conditions. In contrast, the majority of mono-PUFA species did not change beyond 4.4±3.4% with the exception of one species, PE-(18:0/22:4), for which the loss was 21.3±3.2%. These data indicate that di-PUFA-PE species may be acting as a driving force of lipid peroxidation and ferroptotic death. This interpretation is in line with the measurements of lipid peroxidation using an HOO-lipid specific fluorescent probe, LiperFluo, which indicates the intracellular HOO-lipid accumulation.[15,16] This is observed as a robust fluorescent response in cells incubated with RSL3+15LOX-2+di-AA-PE vs RSL3 alone (**Figure 7E**). Similarly, an overall stronger total peroxidation of di-PUFA-PE species containing AA-/AdA-residues was also observed in placental primary human trophoblasts (PHT) (**Supplementary Figure 5**).

To determine how early after the initiation of ferroptosis the loss of oxidizable di-PUFA-PEs vs. mono-PUFA-PEs occurs, we studied the time course of RSL3-induced ferroptotic death of A375 melanoma cells *in vitro*. We observed an almost linear increase in the number of dead cells from 1.4±0.2% to 40.8±3.2% of RSL3 treatment over 3–16 hours (**Figure 8A**). Overall, the relative decrease of di-PUFA-PEs occurred to a markedly greater extent (up to 43.2±3.1%) than in mono-PUFA-PE species, where the loss did not exceed 21.8±2.4% (**Figure 8B**). Most remarkably, the oxidative loss of both di-PUFA-PEs and mono-PUFA-PEs was highly species-specific. For some of the di-PUFA-PE species, the contents did not change early (3-6 h) in the ferroptotic process (20:4/20:4-PE, 20:4/22:5-PE, 20:4/22:6-PE) and became robust after 9-16h of incubation. For several other species, the decreased amounts were observed already at 3h (20:4/22:4-PE, 22:4/22:4-PE), and for some other species (e.g., 22:4/22:6-PE) the changes in their amounts were progressive. This species dependence was also observed for mono-PUFA-PE species with three types of characteristic responses: i) the emergence of oxidative loss of the species very early in the ferroptotic process starting at 3h with only minor changes occurring after this (18:0/20:4-PE, 18:1/20:4, 18:0/22:4-PE), ii) monotonous consumption (16:0/20:4-PE), and iii) lack of any changes in the contents of this species (16:1/20:4-PE). Overall, these data demonstrate, for the first time, a remarkable selectivity of PUFA-PE oxidative loss corresponding to their involvement in the execution of ferroptosis. Different stages of the ferroptotic

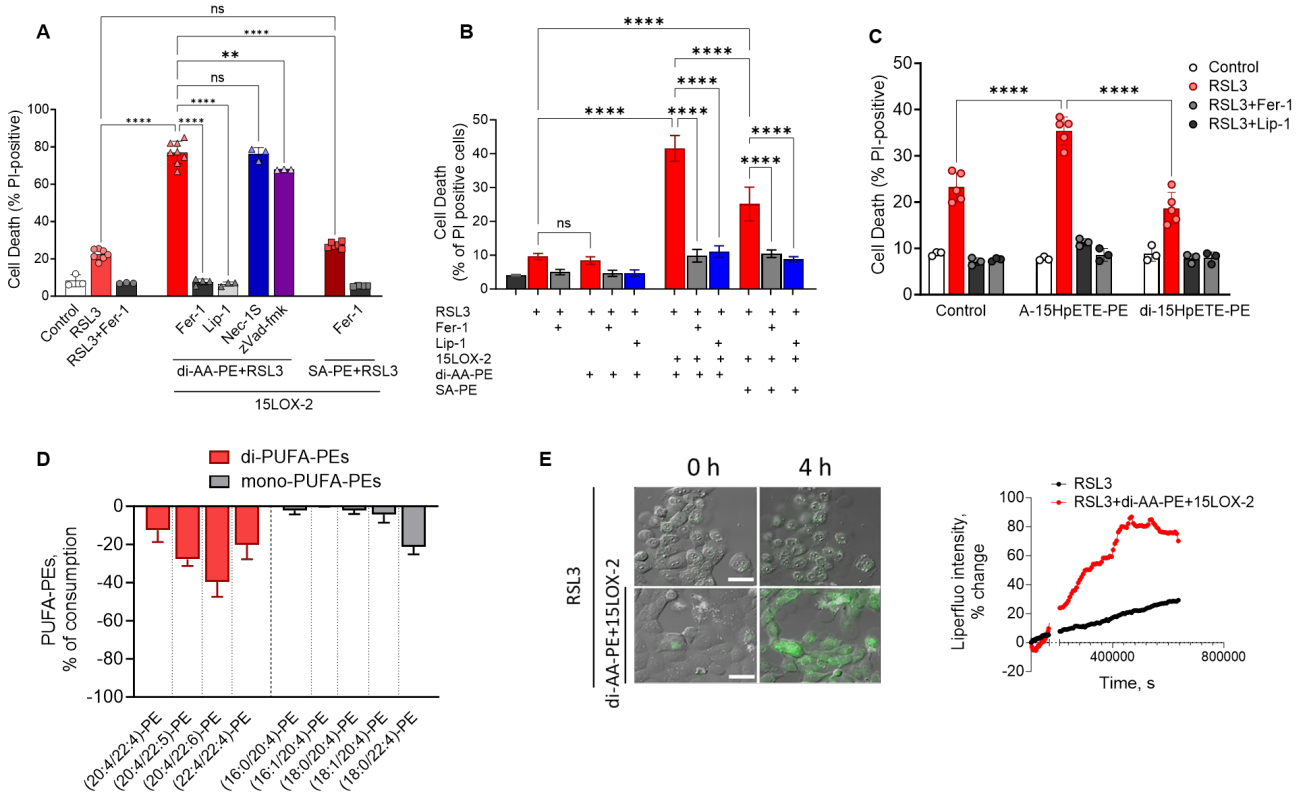

Figure 7. Oxidation of di-AA-PE by 15LOX-2 sensitizes cells to ferroptosis. HBE and HaCaT cells were primed with RSL3 (**A**) HBE (75 nM), (**B**) HaCaT (50 nM) for 3h and then treated with di-AA-PE or SA-PE containing liposomes and 15LOX-2 with or without inhibitors of different cell death pathways – ferroptosis (Fer-1 or Lip-1), necroptosis (Nec-1S), apoptosis (zVAD-fmk). Cell death was analyzed by PI-staining using flow. Data are mean ± s.d., n=3-8, ****p<0.0001, **p<0.01, One-way ANOVA, Tukey's multiple comparisons test. (**C**) HBE cells were primed with RSL3 (75 nM for 3h) and then treated with AA-15HpETE-PE or di-15HpETE-PE. Cell death was analyzed by PI-staining using flow. Data are mean ± s.d., n=3-5, ****p < 0.0001, student's t-test. (**D**) Consumption (%) of di- and mono-PUFA-PEs in HBE cells treated with 15LOX-2 and di-AA-PE and exposed to RSL3 for 4 hours compared to the controls, n=3. (**E**) Detection of lipid hydroperoxides. Live cell fluorescence imaging of Liperfluo in HBE cells treated with RSL3 alone or RSL3+15LOX-2+di-AA-PE. Left panel shows changes in fluorescence in one stage position (of 10) at 0h and 4h. Right panel shows the time course of changes in fluorescence intensity from baseline. Scale bars, 20 μm.

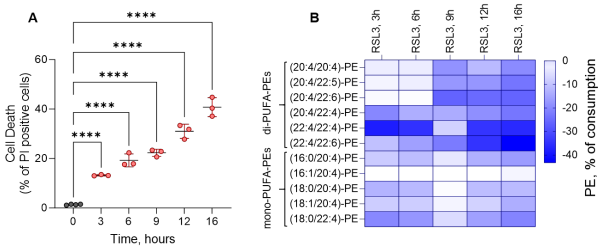

Figure 8. RSL3 induced cell death and consumption of di-PUFA-PE and mono-PUFA-PE species in A375 melanoma cells. **(A)** RSL3 induced cell death in a time-dependent manner as evidenced by PI positive cells. Data are mean ± s.d., n=3-4, ****p<0.0001 vs control, One-way ANOVA, Tukey's multiple comparisons test. **(B)** Consumption of AA-/AdA-containing di-PUFA-PE and mono-PUFA-PE species in cells exposed to RSL3. Data are expressed as % of the substrate loss compared to the controls and presented as a heat map, n = 3.

process are characterized by the engagement of multiple and alternate molecular species of di-PUFA-PEs and mono-PUFA-PEs.

In the ferroptotic models examined (**Figures 7,8**), we were able to detect the accumulation of peroxidation products for some PUFA-PE species where loss was observed, but not in all of them. More specifically, we were able to detect up to 43.2±3.1% losses of (22:4/22:6)-PE and 38.4±1.3% of (22:4/22:4)-PE species (**Figure 8B**). However, no HOO-oxidation products in these species were detectable. This may be due to the conversion of the primary peroxidation products, HOO-PUFA-PEs, into secondary oxidatively-truncated species or covalent adducts with proteins. Indeed, we were able to detect oxidatively-truncated PE species in A375 cells (PE-(18:0/C8-hydroxy-oxo-enoyl)) and HBE cells (PE-(18:0/C7-hydroxy-anoyl), PE-(18:0/C5-oxo-anoyl), PE-(18:1/C5-oxo-anoyl)) primed to ferroptosis. However, for some species, particularly for all di-PUFA-PE species, no detectable amounts of peroxidation and truncated products accumulated. We assumed that the contents of peroxidation products, as transient intermediates of the ferroptotic process, may be dictated by two major specific factors: i) specificity of the initiators of peroxidation, and ii) control of the HOO-PUFA-PE decay to oxidatively-truncated electrophilic species and their reactivity towards forming covalent adducts with proteins.

When A375 melanoma cells were treated with tert-butyl-hydroperoxide (TBH) causing 78.2±0.7% of cell death (**Figure 9A**), we observed a characteristic loss of several AA/AdA-containing di-PUFA-PE substrates (**Figure 9B**) and simultaneous accumulation of HO- and HOO-containing peroxidation products (**Figure 9C**). While very low abundance was typical for some of them, much higher levels of AdA-containing di-PUFA-OOH-PE species (up to 18.2±10.4% mol%) were revealed after incubation with TBH. Under these conditions, oxidative consumption of mono-PUFA-PEs was detectable simultaneously with the accumulation of a variety of different peroxidation products (**Figure 9D,E**). Importantly, both PE peroxidation and cell death were strongly suppressed by Fer-1 indicating the engagement of typical ferroptotic mechanisms (**Figure 9A**).

ACSL4 is a well-known regulator of a cell's sensitivity to pro-ferroptotic stimuli acting through the regulation of

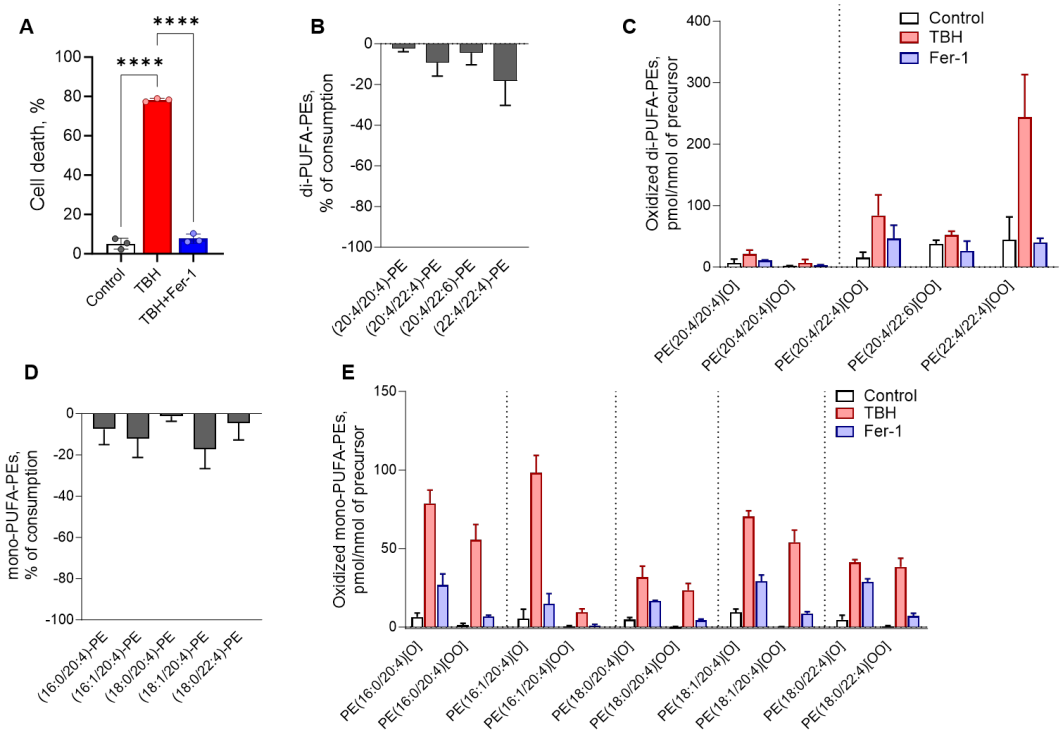

Figure 9. TBH induced cell death, accumulation of PE-derived ferroptotic cell death signals and consumption of di-PUFA-PE and mono-PUFA-PE species in A375 melanoma cells. **(A)** TBH induces cell death as evidenced by Trypan blue staining. Data are mean ± s.d., n=3, **** p<0.0001, One-way ANOVA, Tukey's multiple comparisons test. Consumption (%) of **(B)** di-PUFA-PEs and **(D)** mono-PUFA-PEs in A375 cells exposed to TBH for 6 hours compared to the controls. Data are mean ± s.d., n=3-4. Accumulation of oxidized **(C)** di-PUFA-PEs and **(E)** mono-PUFA-PEs in A375 cells exposed to TBH. Data are expressed as pmol/nmol of precursor. Data are mean ± s.d., n=3-4.

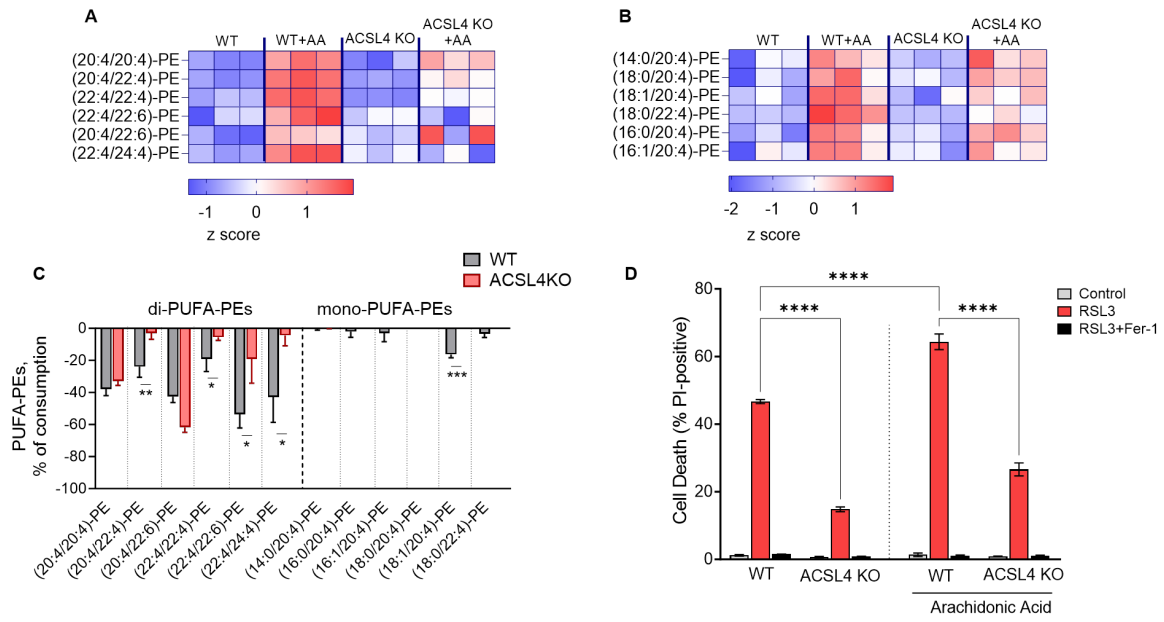

Figure 10. RSL3 induced cell death and consumption of di-PUFA-PE and mono-PUFA-PE species in WT and ACSL4 KO A375 plus/minus AA-supplemented melanoma cells. Content of AA-/AdA-containing **(A)** di-PUFA-PE and **(B)** mono-PUFA-PE species in A375 melanoma obtained from control cells and cells treated with AA. Data are expressed as pmol/nmol of PLs and presented as heat maps auto-scaled to z scores and coded blue (low values) to red (high values), n = 3. **(C)** Consumption of di-PUFA-PE and mono-PUFA-PE species in WT and ACSL4 KO A375 AA-supplemented melanoma cells exposed to RSL3 for 12 hours. Data are expressed as % of the substrate loss compared to the WT+AA or ACSL4 KO+AA conditions. Data are mean ± s.d., n = 3. * p<0.05** p<0.005, *** p<0.0005, student's t-test. **(D)** RSL3 induced cell death in WT and ACSL4 KO A375 plus/minus AA-supplemented cells. Data are mean± s.d., n=3, **** p<0.0001, One-way ANOVA, Tukey's multiple comparisons test.

PUFA-acyl-CoA (particularly arachidonoyl-CoA) and synthesis of PUFA-PLs, particularly after supplementation of cells with AA.[3,17] We asked which of the two types of AA-containing PLs – mono-AA or di-AA-PEs are mostly regulated by ACSL4. To address this experimentally, we used a model of WT and ACSL4 KO A375 plus/minus AA-supplemented cells (**Supplementary Figure 6**). In WT cells, all di-PUFA-PEs universally responded by robustly (1.5-4.0-fold) elevated levels of the respective molecular species to AA supplementation (**Figure 10A**). This stimulation was partially or completely suppressed in ACSL4 KO cells, and the level of suppression was highly PE-species-specific. The ACSL4-dependent increases in mono-PUFA-PEs were overall much lower vs di-PUFA-PE species in both WT and ACSL4 KO cells (**Figure 10B**).

Importantly, pro-ferroptotic stimulation with RSL3 caused strong oxidative loss responses in several di-PUFA-PE species (20:4/20:4-PE and 20:4/22:6-PE) of both WT and ACSL4 KO cells (**Figure 10C**). For four di-PUFA-PE molecular species (20:4/22:4)-PE, (22:4/22:6)-PE, (22:4/24:4)-PE and (22:4/22:4-PE) the oxidation-dependent loss was found to be consequently up to 23.9±5.5%, 53.7±6.9%, 43.0±12.8%, 19.1±6.5% in WT cells and was strongly suppressed for the same species in ACSL4 KO cells. Essentially, no RSL3 induced oxidative loss was found in mono-PUFA-PEs of both WT or ACSL4 KO cells (with the exception of 18:1/20:4-PE species with a 16.3±1.7% loss) (**Figure 10C**). The pro-ferroptotic response to RSL3 treatment of non-AA-supplemented WT cells (46.7±0.5% death) was strongly (>3-fold, 14.8±0.6%) inhibited in ACSL4 KO cells (**Figure 10D**). AA-supplementation expectedly sensitized cells to ferroptosis, but it also "smoothened" the difference between WT and ACSL4 KO cells (~2.4-fold), from 64.4±2.1% cell death in WT to 26.6±1.6% in ACSL4 KO cells. Fer-1 inhibited ferroptotic responses to control levels for both WT and ACSL4 cells in plus/minus AA-supplemented conditions. Overall, these results clearly indicate that not all PUFA-containing PLs contribute equally to ferroptotic death, highlighting the important role of di-PUFA-PEs.

Discussion

Asymmetry of PUFA *vs.* SFA/MUFA distribution between sn1 and sn2 positions of PLs is fundamental for life.[18,19,20] While there are examples of deviations from this important asymmetric organization, they are quite rare. As examples, one can name the formation of di-PUFA PLs as the required substrates in the biosynthesis of N-acyl-PEs,[21] precursors of endocannabinoids, like anandamide,[22] or bis(monoacylglycero)phosphates (BMPs) participating in the regulation of hydrolytic digestion of unnecessary or damaged molecules in the late endo-lysosomal compartment.[23] The presence of non-oxidizable SFA/MUFA acyls is essential for the metabolic engagements of PLs in the membrane.[24] Indeed, if the sn2 PUFA residue is involved in the production of lipid signals, e.g. lipid mediators, the second acyl chain in the sn1-position will still anchor the lyso-PL molecule in the membrane lipid bilayer, thus preserving it for remodeling and further re-use. If both sn1 and sn2 positions are occupied by PUFA-residues, their oxidation or other metabolic involvements will eliminate this PL molecule from the membrane.

Robust PL peroxidation has been universally recognized as a hallmark of ferroptosis.[1,13] However, the most frequently employed analytical methodologies do not permit direct establishment of the identity and amounts of specific PL peroxidation products. LC-MS based redox lipidomics reveals a large diversity of these peroxidized (phospho)lipids, albeit semi-quantitatively, as calibration standards are

available for only a few of them.[7,9,25,26] In spite of that, our study discovered a new role of di-PUFA-PE peroxidation, driven by 15LOX, in the execution of the ferroptotic cell death program. We determined that there are substantial differences in the quantitative participation and time course of the formation, transient accumulation and adduction with proteins of different peroxidation products generated from di-PUFA-PEs and mono-PUFA-PEs. This newly established role of di-PUFA-PEs in ferroptosis emphasizes the necessity of highly effective regulation of their biosynthesis to avoid unwanted accidental cell death. It is also apparent that nutritionally or metabolically induced excessive elevation of di-PUFA-PEs may lead to their rapid enzymatic peroxidation by LOXs, transgressing into cell death.

Results of this work demonstrate that mono-HOO-PE and di-PUFA-PE species are potent inducers of ferroptosis. Our demonstration of the early involvement of specific di-PUFA-PE species in the peroxidation process points to their possible role in the initiation of the ferroptotic process. This necessitates further studies on enzymatic mechanisms involved in the biosynthesis and regulation of di-PUFA-PLs in the cell.

The amazing feature of di-PUFA-PEs is that they can get oxidized at unexpectedly high rates by 15LOX (**Figure 2**). Our MD simulations revealed that this is mainly due to specific orientations of PUFA- vs. SFA/MUFA-PE residues with regards to the 15LOX catalytic iron (**Figure 4,5**). There is a substantial difference in the catalytic competence of di-PUFA-PE oxidation between the two 15LOX isoforms, 15LOX-1 and 15LOX-2 (**Figure 2**). Further studies will reveal the molecular basis underlying these mechanistic differences and their biological role.

While the contents of di-AA-PE and other di-PUFA-PEs are > than an order of magnitude lower than sn-1-SFA/MUFA-sn-2-PUFA-PEs (**Figure 1**), the much higher peroxidation efficiency of di-PUFA-PEs makes their peroxidation possible and demonstrates their significance for the execution of ferroptosis and possibly other functions. For example, canonical biosynthesis of lipid mediators begins with the hydrolysis of PLs and subsequent liberation of PUFA, which then serve as oxidizable precursors.[27] Direct oxidation of di-AA-PE points to a possible alternative pathway for biosynthesis of lipid mediators occurring as a sequential 15-LOX-catalyzed peroxidation of di-PUFA-PLs followed by the hydrolysis of peroxidized di-PUFA-PLs by group VI PLA2 of special types – Ca^{2+}-independent PLA2 - capable of attacking oxidatively modified PL-substrates.[28,29] This mechanism for lipid mediator formation may occur independently of the canonical pathway, which is initiated by the PLA2-mediated liberation of free PUFA from the sn-2-position of PLs.

AUTHOR INFORMATION

Corresponding Authors

*Hülya Bayır: hb2753@cumc.columbia.edu
*Valerian E. Kagan: kagan@pitt.edu

ORCID

Svetlana N Samovich: 0000-0001-5731-122X
Valerian E. Kagan: 0000-0002-7245-1885
Hülya Bayır: 0000-0003-2361-4120
Ivet Bahar: 0000-0001-9959-4176
Karolina Mikulska-Ruminska: 0000-0001-7227-5503
Haider H. Dar: 0000-0001-9586-7288
Yulia Tyurina: 0000-0003-0287-2091
Vladimir Tyurin: 0000-0002-3474-1697
Oleksandr Kapralov: 0000-0002-3006-916X
Andrew Amoscato: 0000-0002-1340-9150

Notes

The authors declare no competing financial interest.

ACKNOWLEDGMENT

This work was supported by the National Institutes of Health grant numbers: AI156924, AI156923, AI145406, HL114453, NS061817, NS076511, CA165065, CA266342, CA243142; Polish National Science Centre grant number: 2019/35/D/ST4/02203.

ABBREVIATIONS

AA, arachidonic acid; ACSL4, acyl coenzyme A synthetase long chain family member 4; AdA, adrenic acid; AA-residue, arachidonoyl-residue; ETE, eicosatetraenoyl; FA, fatty acid; Fer-1, ferrostatin-1; Lip-1, liproxstatin-1; 15LOX, 15-lipoxygenase; MUFA, monounsaturated fatty acid; MD, molecular dynamics; SFA, saturated fatty acid; PE, phosphatidylethanolamine; PEox, oxidized phosphatidylethanolamine; PC, phosphatidylcholine; PUFA-PL, polyunsaturated-fatty-acid-containing phospholipid; PLA2, phospholipase A2; PL, phospholipid; PEBP1, phosphatidylethanolamine binding protein 1; TBH, tert-butyl-hydroperoxide; WT, wild type.

REFERENCES

(1) Dixon, S. J.; Lemberg, K. M.; Lamprecht, M. R.; Skouta, R.; Zaitsev, E. M.; Gleason, C. E.; Patel, D. N.; Bauer, A. J.; Cantley, A. M.; Yang, W. S.; Morrison, B., 3rd; Stockwell, B. R. Ferroptosis: an iron-dependent form of nonapoptotic cell death. *Cell*, **2012**, 149(5), 1060–1072. DOI: 10.1016/j.cell.2012.03.042

(2) Wiernicki, B.; Dubois, H.; Tyurina, Y. Y.; Hassannia, B.; Bayir, H.; Kagan, V. E.; Vandenabeele, P.; Wullaert, A.; Vanden Berghe, T. Excessive phospholipid peroxidation distinguishes ferroptosis from other cell death modes including pyroptosis. *Cell Death Dis.*, **2020**, 11(10), 922. DOI: 10.1038/s41419-020-03118-0

(3) Doll, S.; Proneth, B.; Tyurina, Y. Y.; Panzilius, E.; Kobayashi, S.; Ingold, I.; Irmler, M.; Beckers, J.; Aichler, M.; Walch, A.; Prokisch, H.; Trümbach, D.; Mao, G.; Qu, F.; Bayir, H.; Füllekrug, J.; Scheel, C. H.; Wurst, W.; Schick, J. A.; Kagan, V. E.; Angeli, J. P.; Conrad, M. ACSL4 dictates ferroptosis sensitivity by shaping cellular lipid composition. *Nat. Chem. Biol.*, **2017**, 13(1), 91–98. DOI: 10.1038/nchembio.2239

(4) Kim, R.; Hashimoto, A.; Markosyan, N.; Tyurin, V. A.; Tyurina, Y. Y.; Kar, G.; Fu, S.; Sehgal, M.; Garcia-Gerique, L.; Kossenkov, A.; Gebregziabher, B. A.; Tobias, J. W.; Hicks, K.; Halpin, R. A.; Cvetesic, N.; Deng, H.; Donthireddy, L.; Greenberg, A.; Nam, B.; Vonderheide, R. H.; Nefedova, Y.; Kagan, V. E.; Gabrilovich, D. I. Ferroptosis of tumour neutrophils causes immune suppression in cancer. *Nature*, **2022**, 612(7939), 338–346. DOI: 10.1038/s41586-022-05443-0

(5) Liang, D.; Feng, Y.; Zandkarimi, F.; Wang, H.; Zhang, Z.; Kim, J.; Cai, Y.; Gu, W.; Stockwell, B. R.; Jiang, X. Ferroptosis surveillance independent of GPX4 and differentially regulated by sex hormones. *Cell*, **2023**, 186(13), 2748–2764.e22. DOI: 10.1016/j.cell.2023.05.003

(6) Amoscato, A. A.; Anthonymuthu, T.; Kapralov, O.; Sparvero, L. J.; Shrivastava, I. H.; Mikulska-Ruminska, K.; Tyurin, V. A.; Shvedova, A. A.; Tyurina, Y. Y.; Bahar, I.; Wenzel, S.; Bayir, H.; Kagan, V. E. Formation of protein adducts with Hydroperoxy-PE electrophilic cleavage products during ferroptosis. *Redox. Biol.*, **2023**, 63, 102758. DOI: 10.1016/j.redox.2023.102758

(7) Tyurina, Y. Y.; Kapralov, A. A.; Tyurin, V. A.; Shurin, G.; Amoscato, A. A.; Rajasundaram, D.; Tian, H.; Bunimovich, Y. L.; Nefedova, Y.; Herrick, W. G.; Parchment, R. E.; Doroshow, J. H.; Bayir, H.; Srivastava, A. K.; Kagan, V. E. Redox phospholipidomics discovers pro-ferroptotic death signals in A375 melanoma cells in vitro and in vivo. *Redox. Biol.*, **2023**, 61, 102650. DOI: 10.1016/j.redox.2023.102650

(8) Yang, W. S.; Kim, K. J.; Gaschler, M. M.; Patel, M.; Shchepinov, M. S.; Stockwell, B. R. Peroxidation of polyunsaturated fatty acids by lipoxygenases drives ferroptosis. *PNAS*, **2016**, 113(34), E4966–E4975. DOI: 10.1073/pnas.1603244113

(9) Wenzel, S. E.; Tyurina, Y. Y.; Zhao, J.; St Croix, C. M.; Dar, H. H.; Mao, G.; Tyurin, V. A.; Anthonymuthu, T. S.; Kapralov, A. A.; Amoscato, A. A.; Mikulska-Ruminska, K.; Shrivastava, I. H.; Kenny, E. M.; Yang, Q.; Rosenbaum, J. C.; Sparvero, L. J.; Emlet, D. R.; Wen, X.; Minami, Y.; Qu, F.; Watkins S. C.; Holman T. R.; VanDemark A. P.; Kellum J. A.; Bahar I.; Bayır H.; Kagan, V. E. PEBP1 Wardens Ferroptosis by Enabling Lipoxygenase Generation of Lipid Death Signals. *Cell*, **2017**, 171(3), 628–641.e26. DOI: 10.1016/j.cell.2017.09.044

(10) Kuhn, H.; Banthiya, S.; van Leyen, K. Mammalian lipoxygenases and their biological relevance. *Biochim Biophys Acta*, **2015**, 1851(4), 308–330. DOI: 10.1016/j.bbalip.2014.10.002

(11) Kuhn, H.; O'Donnell, V. B. Inflammation and immune regulation by 12/15-lipoxygenases. *Prog. Lipid Res.*, **2006**, 45(4), 334–356. DOI: 10.1016/j.plipres.2006.02.003

(12) Kuhn, H.; Humeniuk, L.; Kozlov, N.; Roigas, S.; Adel, S.; Heydeck, D. The evolutionary hypothesis of reaction specificity of mammalian ALOX15 orthologs. *Prog. Lipid Res.*, **2018**, 72, 55–74. DOI: 10.1016/j.plipres.2018.09.002

(13) Yang, W. S.; Stockwell, B. R. Ferroptosis: Death by Lipid Peroxidation. *Trends Cell. Biol.*, **2016**, 26(3), 165–176. DOI: 10.1016/j.tcb.2015.10.014

(14) Yang, W. S.; Stockwell, B. R. Synthetic lethal screening identifies compounds activating iron-dependent, nonapoptotic cell death in oncogenic-RAS-harboring cancer cells. *Chem. Biol.*, **2008**, 15(3), 234–245. DOI: 10.1016/j.chembiol.2008.02.010

(15) Li, B.; Pratt, D. A. Methods for determining the efficacy of radical-trapping antioxidants. *Free Radic. Biol. Med.*, **2015**, 82, 187–202. DOI: 10.1016/j.freeradbiomed.2015.01.020

(16) Yamanaka, K.; Saito, Y.; Sakiyama, J.; Ohuchi, Y.; Osetob, F.; Noguchi, N. A novel fluorescent probe with high sensitivity and selective detection of lipid hydroperoxides in cells. *RSC Adv.,* **2012**, 2, 7894–7900. DOI: 10.1039/C2RA20816D

(17) Zhang, H. L.; Hu, B. X.; Li, Z. L.; Du, T.; Shan, J. L.; Ye, Z. P.; Peng, X. D.; Li, X.; Huang, Y.; Zhu, X. Y.; Chen, Y. H.; Feng, G. K.; Yang, D.; Deng, R.; Zhu, X. F. PKCβII phosphorylates ACSL4 to amplify lipid peroxidation to induce ferroptosis. *Nat. Cell Biol.*, **2022**, 24(1), 88–98. DOI: 10.1038/s41556-021-00818-3

(18) Manni, M. M; Tiberti, M. L; Pagnotta, S.; Barelli, H.; Gautier, R.; Antonny, B. Acyl chain asymmetry and polyunsaturation of brain phospholipids facilitate membrane vesiculation without leakage. *eLife*, **2018**, 7, e34394. DOI: 10.7554/eLife.34394

(19) Pinot, M.; Vanni, S.; Pagnotta, S.; Lacas-Gervais, S.; Payet, L. A.; Ferreira, T.; Gautier, R.; Goud, B.; Antonny, B.; Barelli, H. Lipid cell biology. Polyunsaturated phospholipids facilitate membrane deformation and fission by endocytic proteins. *Science*, **2014**, 345(6197), 693–697. DOI: 10.1126/science.1255288

(20) Vásquez, V.; Krieg, M.; Lockhead, D.; Goodman, M. B. Phospholipids that contain polyunsaturated fatty acids enhance neuronal cell mechanics and touch sensation. *Cell reports*, **2014**, 6(1), 70–80. DOI: 10.1016/j.celrep.2013.12.012

(21) Ueda, N.; Tsuboi, K.; Uyama, T. Enzymological studies on the biosynthesis of N-acylethanolamines. *BBA*, **2010**, 1801(12), 1274–1285. DOI: 10.1016/j.bbalip.2010.08.010

(22) Astarita, G.; Ahmed, F.; Piomelli, D. Identification of biosynthetic precursors for the endocannabinoid anandamide in the rat brain. *J. Lipid Res.*, **2008**, 49(1), 48–57. DOI: 10.1194/jlr.M700354-JLR200

(23) Showalter, M. R.; Berg, A. L.; Nagourney, A.; Heil, H.; Carraway, K. L. 3rd; Fiehn, O. The emerging and diverse roles of bis(monoacylglycero) phosphate lipids in cellular physiology and disease. *Int. J. Mol. Sci.*, **2020**, 21(21), 8067. DOI: 10.3390/ijms21218067

(24) Hitaishi, P.; Mandal, P.; Ghosh, S. K. Partitioning of a hybrid lipid in domains of saturated and unsaturated lipids in a model cellular membrane. *ACS omega*, **2021**, 6(50), 34546–34554. DOI: 10.1021/acsomega.1c04835

(25) Kagan, V. E.; Tyurina, Y. Y.; Vlasova, I. I.; Kapralov, A. A.; Amoscato, A. A.; Anthonymuthu, T. S.; Tyurin, V. A.; Shrivastava, I. H.; Cinemre, F. B.; Lamade, A.; Epperly, M. W.; Greenberger, J. S.; Beezhold, D. H.; Mallampalli, R. K.; Srivastava A. K.; Bayir, H.; Shvedova, A. A. Redox epiphospholipidome in programmed cell death signaling: catalytic mechanisms and regulation. *Front. Endocrinol.*, 11, **2021**, 628079. DOI: 10.3389/fendo.2020.628079

(26) Tyurina, Y. Y.; Tyurin, V. A.; Anthonymuthu, T.; Amoscato, A. A.; Sparvero, L. J.; Nesterova, A. M.; Baynard, M. L.; Sun, W.; He, R.; Khaitovich, P.; Vladimirov, Y. A.; Gabrilovich, D. I.; Bayır, H.; Kagan, V. E. "Redox lipidomics technology: Looking for a needle in a haystack". *Chem. Phys. Lipids*, **2019**, 221, 93–107. DOI: 10.1016/j.chemphyslip.2019.03.012

(27) Hirabayashi, T.; Murayama, T.; Shimizu, T. Regulatory mechanism and physiological role of cytosolic phospholipase A2. *Biol. Pharm. Bull.*, **2004**, 27(8):1168–73. DOI: 10.1248/bpb.27.1168

(28) Sun, W. Y.; Tyurin, V. A.; Mikulska-Ruminska, K.; Shrivastava; I. H.; Anthonymuthu, T. S.; Zhai, Y. J.; Pan, M. H.; Gong, H. B.; Lu, D. H.; Sun, J.; Duan, W. J.; Korolev, S.; Abramov, A. Y.; Angelova, P. R.; Miller, I.; Beharier, O.; Mao, G. W.; Dar, H. H.; Kapralov, A. A.; Amoscato, A. A.; Hastings, T. G.; Greenamyre T. J.; Chu, C.T.; Sadovsky, Y.; Bahar, I., Bayır, H.; Tyurina, Y. Y.; He, R. R.; Kagan, V. E. Phospholipase iPLA2β averts ferroptosis by eliminating a redox lipid death signal. *Nat. Chem. Biol.*, **2021**, 17(4), 465–476. DOI: 10.1038/s41589-020-00734-x

(29) Liu, G. Y.; Moon, S. H.; Jenkins, C. M.; Li, M.; Sims, H. F.; Guan, S.; Gross, R. W. The phospholipase iPLA2γ is a major mediator releasing oxidized aliphatic chains from cardiolipin, integrating mitochondrial bioenergetics and signaling. *J. Biol. Chem.,* **2017**, 292, 10672–10684. DOI: 10.1074/jbc.M117.783068